

# Interpreting the First CMS and ATLAS SUSY Results

Sujeet Akula,<sup>1</sup> Ning Chen,<sup>2</sup> Daniel Feldman,<sup>3</sup> Mengxi Liu,<sup>1</sup> Zuowei Liu,<sup>2</sup> Pran Nath,<sup>1</sup> and Gregory Peim<sup>1</sup>

<sup>1</sup>*Department of Physics, Northeastern University, Boston, MA 02115, USA*

<sup>2</sup>*C.N. Yang Institute for Theoretical Physics, Stony Brook University, Stony Brook, NY 11794, USA*

<sup>3</sup>*Michigan Center for Theoretical Physics, University of Michigan, Ann Arbor, MI 48109, USA*

The CMS and the ATLAS Collaborations have recently reported on the search for supersymmetry with  $35 \text{ pb}^{-1}$  of data and have put independent limits on the parameter space of the supergravity unified model with universal boundary conditions at the GUT scale for soft breaking, i.e., the mSUGRA model. We extend this study by examining other regions of the mSUGRA parameter space in  $A_0$  and  $\tan\beta$ . Further, we contrast the reach of CMS and ATLAS with  $35 \text{ pb}^{-1}$  of data with the indirect constraints, i.e., the constraints from the Higgs boson mass limits, from flavor physics and from the dark matter limits from WMAP. Specifically it is found that a significant part of the parameter space excluded by CMS and ATLAS is essentially already excluded by the indirect constraints and the fertile region of parameter space has yet to be explored. We also emphasize that gluino masses as low as 400 GeV but for squark masses much larger than the gluino mass remain unconstrained and further that much of the hyperbolic branch of radiative electroweak symmetry breaking, with low values of the Higgs mixing parameter  $\mu$ , is essentially untouched by the recent LHC analysis.

Keywords: **CMS, ATLAS, LHC, SUGRA GUT**

## I. INTRODUCTION

A candidate model for new physics is the  $N = 1$  supergravity grand unified model [1] which with universal boundary conditions for soft breaking at the unification scale is the model mSUGRA [1–3] (for reviews see [4–6]) defined by the parameter space  $m_0, m_{1/2}, A_0, \tan\beta$  and the sign of  $\mu$ , as well as  $M_G$  and  $\alpha_G$  where  $M_G$  is the grand unification scale and  $\alpha_G$  is the common value of  $\alpha_1, \alpha_2, \alpha_3$  ( $\alpha_i = g_i^2/(4\pi)$ ) and  $g_i$  is gauge coupling) for the gauge groups  $U(1) \times SU(2)_L \times SU(3)_C$  at the unification scale. This model has recently been investigated at the LHC with R parity conservation, and constraints on the model have been set with  $35 \text{ pb}^{-1}$  of data by the CMS and ATLAS collaborations [7–9]. These works, therefore, produce the first direct constraints on supergravity unified models at the LHC. Indeed the recent results of CMS and ATLAS [7–9] are encouraging as they report to surpass the parameter space probed in previous [10] direct searches by LEP and by the Tevatron.

In this work we explore and interpret further the recent data from the LHC in the framework of mSUGRA. In our analysis we follow the techniques developed in Ref. [11], and we study the parameter space under full simulation of the 7 TeV standard model backgrounds [12–16]. The ATLAS analysis produces a reach which is more stringent than the one from CMS and thus in our analysis we utilize the cuts used by ATLAS. For the case  $A_0 = 0$  and  $\tan\beta = 3$  our results are in conformity with the ATLAS results but we explore other regions of the parameter space in  $A_0 - \tan\beta$  plane and discuss the reach plots for these. We also carry out a detailed comparison of the constraints arising from the CMS and ATLAS reach plots [7–9] vs the constraints arising from the Higgs mass lower limits, from flavor physics and specifically from  $\mathcal{B}r(b \rightarrow s\gamma)$  experimental bounds, and from the WMAP relic density constraints on dark matter.

## II. REACH PLOTS WITH $35 \text{ pb}^{-1}$ OF DATA

The ATLAS collaboration has released two analyses, one with 1 lepton [8] and the other with 0 leptons [9] both of which are considered in our analysis. For the 1 lepton analysis we follow the selection requirements that ATLAS reports in [8]. The preselection requirements for events are that a jet must have  $p_T > 20 \text{ GeV}$  and  $|\eta| < 2.5$ , electrons must have  $p_T > 20 \text{ GeV}$  and  $|\eta| < 2.47$  and muons must have  $p_T > 20 \text{ GeV}$  and  $|\eta| < 2.4$ . Further, we veto the “medium” electrons<sup>1</sup> in the electromagnetic calorimeter transition region,  $1.37 < |\eta| < 1.52$ . An event is considered if it has a single lepton with  $p_T > 20 \text{ GeV}$  and its three hardest jets have  $p_T > 30 \text{ GeV}$ , with the leading jet having  $p_T > 60 \text{ GeV}$ . The distance,  $\Delta R = \sqrt{(\Delta\eta)^2 + (\Delta\phi)^2}$ , between each jet with the lepton must satisfy  $\Delta R(j_i, \ell) > 0.4$ , and events are rejected if the reconstructed missing energy,  $\cancel{E}_T$ , points in the direction of any of the three leading

<sup>1</sup> See [32] for a definition of “loose”, “medium” and “tight” electrons

jets,  $\Delta\phi(j_i, \cancel{E}_T) > 0.2$ . Events are then classified into 2 channels, depending on whether the lepton is a muon or an electron. These are then further classified into four regions based on the missing energy and  $m_T$  cuts, where we reconstruct the missing transverse momentum using the selected lepton plus jets with  $p_T > 20$  GeV and  $|\eta| < 4.9$  following ATLAS analysis, and  $m_T = \sqrt{2p_T(\ell) \cancel{E}_T (1 - \cos(\Delta\phi(\ell, \cancel{E}_T)))}$  is the transverse mass between the lepton and the missing transverse momentum vector. The four regions alluded to above are labeled the “signal region”, the “top region”, the “W region” and the “QCD region”. For the “signal region” events were required to pass the additional cuts of  $m_T > 100$  GeV,  $\cancel{E}_T > 125$  GeV,  $\cancel{E}_T > 0.25m_{\text{eff}}$  and  $m_{\text{eff}} > 500$  GeV. Here the effective mass,  $m_{\text{eff}}$ , is the scalar sum of the missing energy with the  $p_T$ 's of the selected visible objects (in this case the lepton and the 3 jets). The number of events were then compared to the 95% CL upper bounds that ATLAS found ( $N_e < 2.2$  events and  $N_\mu < 2.5$  events) [8]. The “top region” and “W region” are defined by events with  $30 \text{ GeV} < \cancel{E}_T < 80 \text{ GeV}$  and  $40 \text{ GeV} < m_T < 80 \text{ GeV}$ , where the “top region” requires at least one of the three hardest jets to be  $b$ -tagged and the “W region” requires none of the three hardest jets to be  $b$ -tagged. The “QCD region” was required to have  $m_T, \cancel{E}_T < 40 \text{ GeV}$  and was purely data driven. For our analysis events were rejected if they contaminated the three control regions. Using the standard model background from [13] we reproduced the ATLAS results.

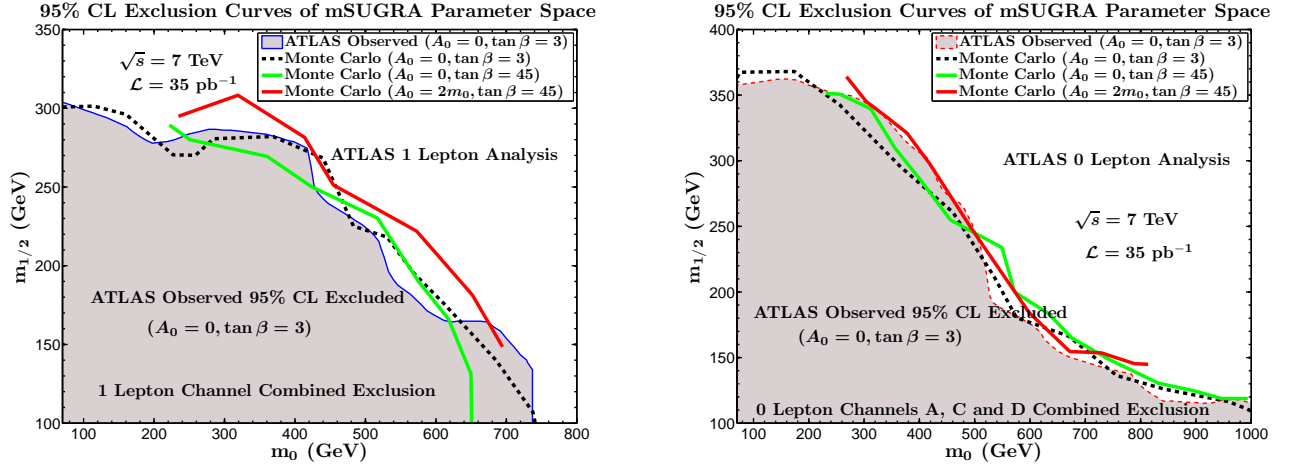


FIG. 1: (color online) Left: Reach plot with  $35 \text{ pb}^{-1}$  of integrated luminosity using the ATLAS cuts [8] [9] with different  $\tan\beta$  and  $A_0$ :  $A_0 = 0$  and  $\tan\beta = 3$  (dashed line);  $A_0 = 0$  and  $\tan\beta = 45$  (solid green line);  $A_0 = 2m_0$  and  $\tan\beta = 45$  (solid red line). For comparison we give the ATLAS observed limit ( $A_0 = 0$  and  $\tan\beta = 3$ ) (solid blue line). Right: Reach plot with  $35 \text{ pb}^{-1}$  of integrated luminosity of data using the ATLAS 0 lepton cuts. For comparison we give the ATLAS observed limit (red dashed line).

For the 0 lepton analysis we follow the selection requirements that ATLAS reports in [9] where the pre-event selection is the same as for the 1 lepton case except that leptons are identified to have  $p_T > 10$  GeV. Here the events are classified into 4 regions “A”, “B”, “C” and “D”; where regions A and B have at least 2 jets and regions C and D have at least 3 jets. When referring to different cuts in these regions we define cuts on the “selected” jets to mean that the bare minimum number of jets in this region must satisfy the following requirement: For regions A and B “selected” jets mean that they are the first two hardest jets and for regions C and D “selected” jets mean that they are the first three hardest jets. Events are required to have  $\cancel{E}_T > 100$  GeV and the selected jets must each have  $p_T > 40$  GeV with the leading jet  $p_T > 120$  GeV. As in the case with 1 lepton, events are rejected if the missing energy points in the direction of any of the selected jets,  $\Delta\phi(j_i, \cancel{E}_T) > 0.4$ , where  $i$  is over the selected jets. Region A requires events to have  $\cancel{E}_T > 0.3m_{\text{eff}}$  and  $m_{\text{eff}} > 500$  GeV and regions C and D require events to have  $\cancel{E}_T > 0.25m_{\text{eff}}$  with region C requiring  $m_{\text{eff}} > 500$  GeV and region D requiring  $m_{\text{eff}} > 1 \text{ TeV}$ . In this case  $m_{\text{eff}}$  is defined in terms of selected jets, i.e. for regions A and B it is the scalar sum of the first two hardest jets and for regions C and D it is the scalar sum of the first three hardest jets. For the analysis here we do not apply the cut for region B, i.e.  $m_{T2} > 300$  GeV, since the models excluded in this region are already excluded in region D [25].

Following the framework of the ATLAS Collaboration [8] we have carried out a set of three parameter sweeps in the  $m_0 - m_{1/2}$  plane taking  $m_{1/2} \leq 500$  GeV and  $m_0 \leq 1 \text{ TeV}$ . Two of the parameter sweeps were a  $10 \text{ GeV} \times 10 \text{ GeV}$  grid scan in the  $m_0 - m_{1/2}$  plane having a fixed universal trilinear parameter,  $A_0 = 0$ , and fixed  $\tan\beta$ ; one set with  $\tan\beta = 3$  and the other with  $\tan\beta = 45$ . A third parameter scan was done with  $A_0 = 2m_0$  and  $\tan\beta = 45$ . Throughout the analysis we take  $\mu > 0$  and  $m_{\text{top}}^{\text{pole}} = 173.1 \text{ GeV}$ . For the simulation of the mSUGRA models, renormalization group evolution and computation of the physical masses of the sparticles was performed using **SuSpect** [22] and we

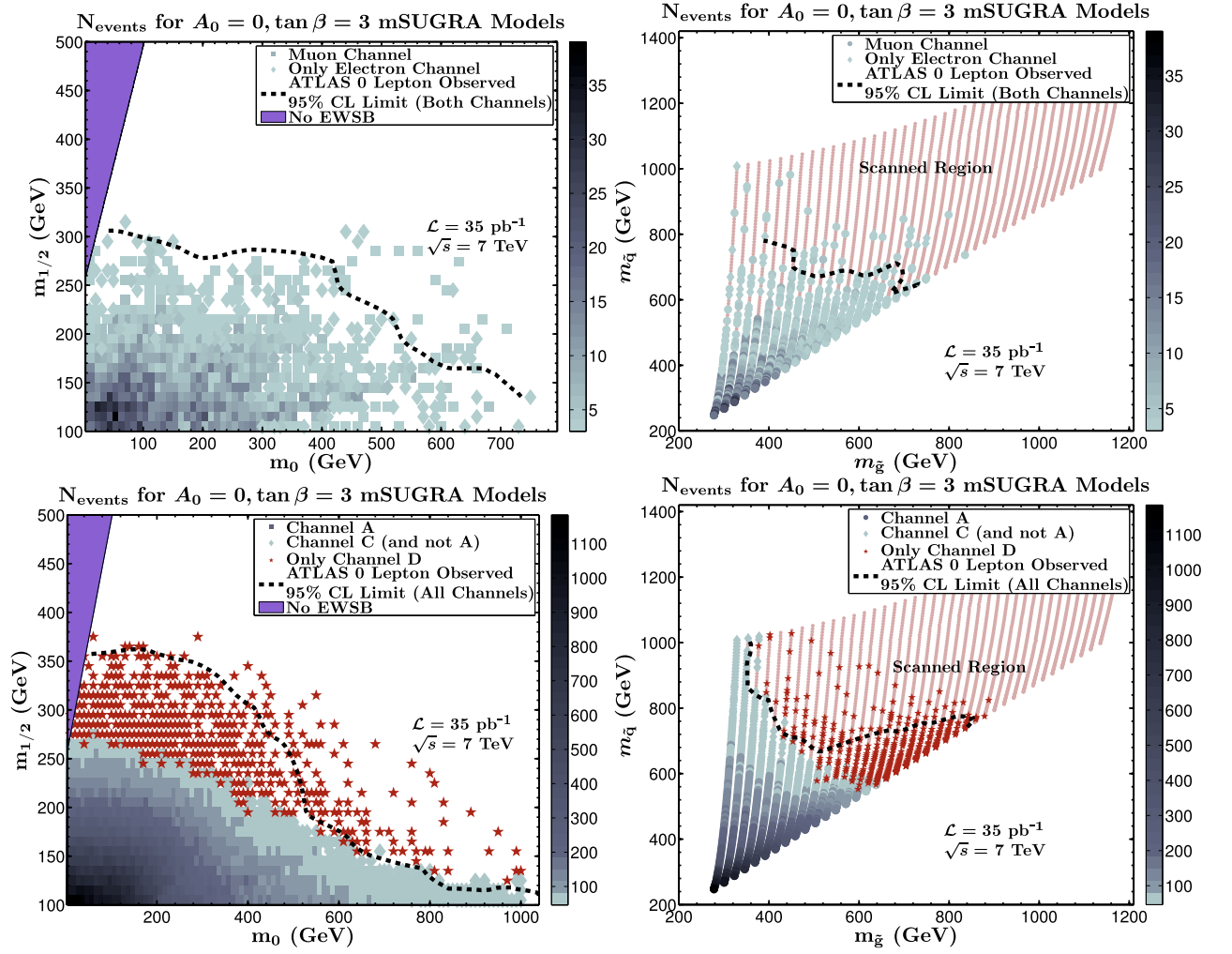


FIG. 2: (color online) Top left panel: Number of signal events in the  $m_0 - m_{1/2}$  plane for the case  $A_0 = 0, \tan \beta = 3$  using the 1 lepton ATLAS cuts in the  $m_0 - m_{1/2}$  plane. The dark areas correspond to number of events greater than 2 with the actual numbers indicated along the vertical line to the right while the white areas are filled with models but have number of events less than 2. Top right panel: Same as the left panel except that the plot is  $m_{\tilde{g}}(\text{gluino}) - m_{\tilde{q}}(\text{squark})$  mass plane for the lightest squark of the first 2 generations. The square region in the left panel becomes squeezed into the polygon-like region in the physical mass plane in the right panel. One may note that the ATLAS constraints do not rule out a low mass gluino on the scale of order 400 GeV for heavy squarks. Bottom left panel: The same as the top left panel except that the analysis is done using 0 lepton ATLAS cuts. Bottom right panel: Same as the top right panel except that the analysis is done using the 0 lepton ATLAS cuts. The (red) stars correspond to channel D. In channel D we find maximally 51 events over the space scanned after a requirement that the number of events be at least 15 before cuts. However, when only considering models not already excluded by channels A and C, the number of events in channel D is maximally 18.

implement both **MadGraph** and **Pythia** for event generation [17, 18]. A comparison of our reach to the reach done by the ATLAS Collaboration is shown in Fig.(1).

In Figure 2 we plot the number of signal events for electrons in the  $m_0 - m_{1/2}$  plane where the reach plot from ATLAS is also exhibited and where the ATLAS reach plot corresponds to the number of observed events and those that have a larger number predicted by the model. For the 1 lepton analysis, we first present the models excluded by the muon channel, colored by  $N_{\text{events}}^{\mu}$  (indicated by squares). Next, we overlay from the remaining models, those that have been excluded by the electron channel, and colored by  $N_{\text{events}}^e$  (indicated by diamonds). Similarly for the 0 lepton analysis, we begin with models excluded by channel A, colored by  $N_{\text{events}}^A$  (indicated by squares); overlay models excluded by C (but not A) and colored by  $N_{\text{events}}^C$  (indicated by diamonds). Next, we overlay models excluded by channel D alone in a single color (stars), as  $N_{\text{events}}^D$  are not comparable with  $N_{\text{events}}^A$  or  $N_{\text{events}}^C$ . We also show the number of signal events for electrons in the  $m_{\tilde{g}} - m_{\tilde{q}}$  plane. An ATLAS reach curve is also exhibited.

The upper left panel of Fig.(2) gives us a more quantitative description of the electron and muon channels in putting constraints on the  $m_0 - m_{1/2}$  parameter space with  $35 \text{ pb}^{-1}$  of data. As expected the largest number of single  $e$  and  $\mu$  events arise at low mass scales, i.e., for low values of  $m_0$  and of  $m_{1/2}$  and the number of signal events decrease and we approach the boundary after which they fall below 2 for the 1 lepton ATLAS analysis. It is also instructive to examine the signal events in the gluino-squark mass plane where the squark mass corresponds to the average first two generation squark mass. This is done in the upper right panel of Fig.(2). Here the polygon shape of the region is a simple mapping of the allowed parameter in the  $m_0 - m_{1/2}$  plane of the upper left panel. The plot is useful as it directly correlates squark and gluino model points that are either excluded or allowed by the 1 lepton ATLAS analysis. The 0 lepton analysis of the lower panels in Fig.(2) is very similar to the analysis of the upper panels except for different array of cuts. There is a general consistency in the analysis of the 1 lepton and the 0 lepton analysis, although the 0 lepton cuts appear more constraining as they appear to exclude a somewhat larger region of the parameter space. Together the analysis of the upper and lower panels of Fig.(2) gives us a more analytical understanding of the relative strengths of the 1 lepton and 0 lepton cuts.

### III. IMPLICATIONS OF CONSTRAINTS

In the analysis of the reach plots experimental constraints were not imposed beyond those that arise from the ATLAS analyses. Next we include these constraints and in our analysis we will consider the larger parameter space when all four parameters  $m_0, m_{1/2}, A_0, \tan \beta$  are varied. In doing so, we apply various constraints from searches on the sparticle mass limits, B-physics and from  $g_\mu - 2$ . Next we explore the constraint from upper bound on the relic density from WMAP only, and then with combination of all of the above. These indirect constraints were calculated using *MicrOmegas* [21], with the Standard Model contribution in the  $\mathcal{B}r(b \rightarrow s\gamma)$  corrected using the NNLO analysis of Misiak *et al.* [28, 30]. We now describe this more general analysis. In the upper left panel of Fig.(3) we apply the following “collider/flavor constraints” [24]  $m_h > 93.5 \text{ GeV}$ ,  $m_{\tilde{\tau}_1} > 81.9 \text{ GeV}$ ,  $m_{\tilde{\chi}_1^\pm} > 103.5 \text{ GeV}$ , and  $m_{\tilde{t}_1} > 100 \text{ GeV}$ , along with  $(-11.4 \times 10^{-10}) \leq \delta(g_\mu - 2) \leq (9.4 \times 10^{-9})$ , see [26],  $\mathcal{B}r(B_s \rightarrow \mu^+ \mu^-) \leq 4.7 \times 10^{-8}$  (90 % C.L.) [29], and  $(2.77 \times 10^{-4}) \leq \mathcal{B}r(b \rightarrow s\gamma) \leq (4.27 \times 10^{-4})$  [27]. These collider/flavor constraints by themselves have an effect, but the effect is quite small in terms of reducing the density of models that are already constrained by the ATLAS results.

We note that our scans of the parameter are very dense with  $10^6$  models after EWSB alone. In the  $m_0 - m_{1/2}$  plane the collider/flavor cuts eliminate 12 % of the models. However because  $A_0$  and  $\tan \beta$  are not fixed to specific values, but are allowed to run over their full natural ranges, a model point which is eliminated for say, large  $\tan \beta$  by  $b \rightarrow s\gamma$  or  $B_s \rightarrow \mu^+ \mu^-$  at a specific point in the  $m_0 - m_{1/2}$  plane can correspond to a model point with a smaller value of  $\tan \beta$  for the same  $(m_0, m_{1/2})$  which is not eliminated. Thus the  $m_0 - m_{1/2}$  plane appears densely filled. This is contrary to what one would observe for fixed values of  $(A_0, \tan \beta)$ . For example, for  $(A_0, \tan \beta) = (0, 45)$  the  $b \rightarrow s\gamma$  constraint would remove models at large  $m_0$  up to close to 2 TeV and  $m_{1/2}$  up to about 750 GeV. As another example, for  $(A_0, \tan \beta) = (0, 3)$  (the space looked at by ATLAS, and in the previous section) a strict limit of  $m_h < 102 \text{ GeV}$  for light CP even Higgs removes all model points below the ATLAS limits. However because one is varying  $(A_0, \tan \beta)$  the area below the ATLAS limit is filled in this case.

Continuing on we next consider the “cosmological constraint” in the upper right panel of Fig.(3) where we apply only an upper bound on the relic density of the thermally produced neutralino dark matter of  $\Omega h^2 \leq 0.14$  [31]. The WMAP upper bound constraint removes 96.5 % of the models alone, thus this cosmological constraint is very severe eliminating a large fraction of models, but again the ATLAS constraints remain quite strong.

Next we consider the “combined collider/flavor and cosmological constraints” and find that together these constraints are generally much more severe than the ATLAS constraints. This is shown in the lower left panel of Fig.(3). Here models that were separately allowed by previously known collider/flavor constraints, and models that were separately allowed by just the upper bound from WMAP, are now eliminated under the imposition of the combined constraints. There is, however, a new region that ATLAS appears to exclude above and beyond what the indirect constraints exclude and this region is a region for low  $m_0$  and for  $m_{1/2}$  around 350 GeV. Thus it would require a larger integrated luminosity to move past the barren region, which is above the ATLAS bound, to get into the fertile region of the parameter space, where the fertile region is the area above the white patch in the lower panel of Fig.(3).

Finally in lower right panel of Fig.(3) we show the value of  $\mu$  (at the electroweak symmetry breaking scale) in the  $m_{1/2} - m_0$  plane where  $\mu$  is the Higgsino mass parameter that enters in the Higgs bilinear term in the superpotential. The analysis is given under the “combined constraints” discussed in the lower left panel of Fig.(3). We note that essentially all of the natural region of the parameter space corresponding to small  $\mu$ , most of which lies close to the hyperbolic branch (Focus point) (HB/FP) [33] of radiative breaking of the electroweak symmetry or near the vicinity of the light CP even Higgs pole region [35] remains untouched by the CMS and LHC exclusion limits as illustrated in the lower right panel of Fig.(3) and remains to be explored. Further, as pointed out in Ref. (1) of [34], low mass

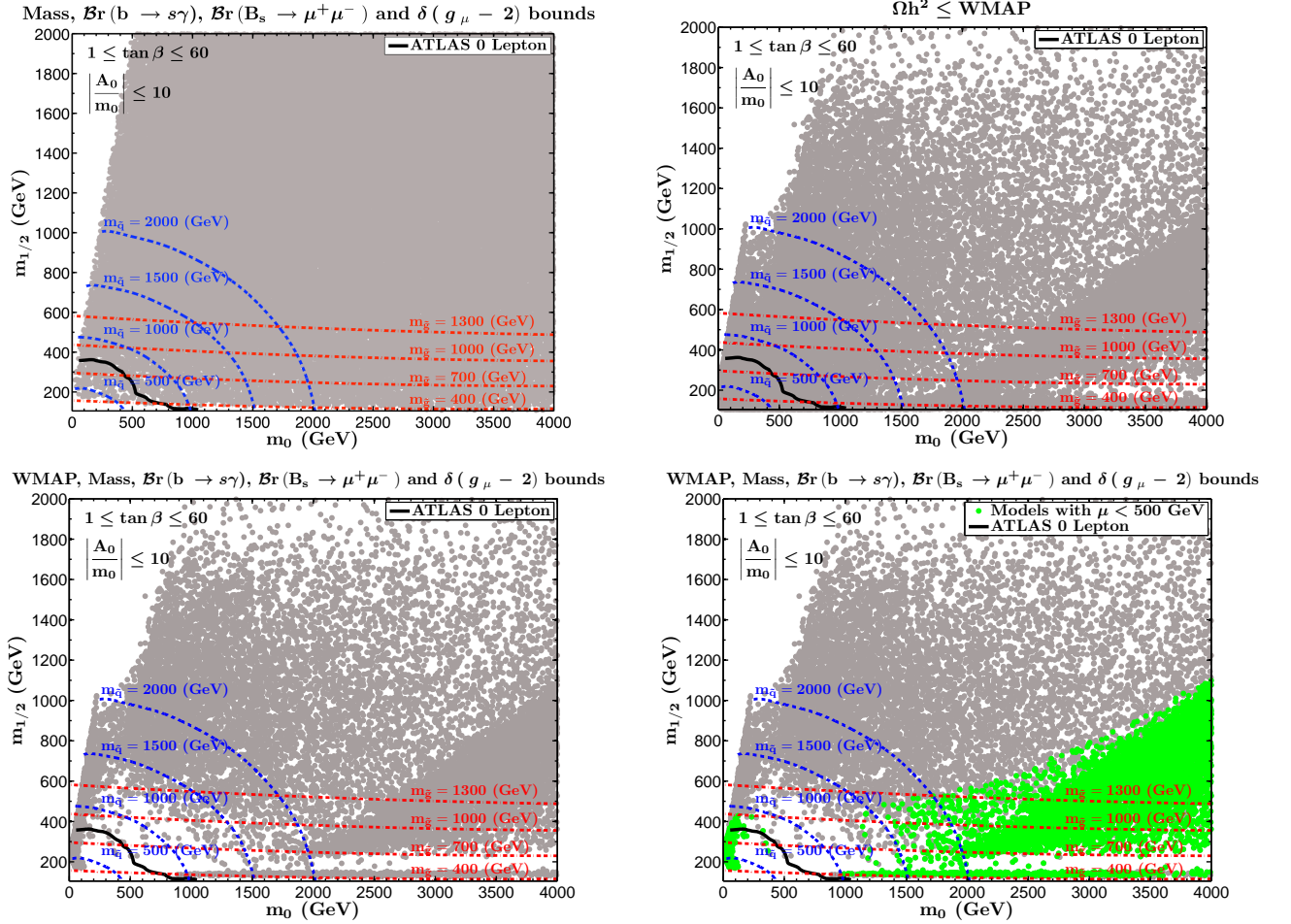


FIG. 3: (color online) Upper left panel: An exhibition of the allowed models indicated by grey (dark) dots in the  $m_0 - m_{1/2}$  plane when only flavor and collider constraints are imposed. The region excluded by ATLAS (as well as CMS) lies below the thick black curve in the left hand corner. Upper right panel: same as the left upper panel except that only an upper bound on relic density of  $\Omega h^2 \leq 0.14$  is imposed. Lower left panel: Same as the upper left panel except that the relic density constraint as in the upper right panel is also applied. This panel exhibits that most of the parameter space excluded by ATLAS is already excluded by the collider/flux and relic density constraints. The dark region below the ATLAS curve is the extra region excluded by ATLAS which was not previously excluded by the indirect constraints. Lower right panel: The analysis of this figure is similar to the lower left panel except that models with  $|\mu| < 500$  GeV are exhibited in green.

gluinos as low as even 420 GeV in mSUGRA are allowed for the region for large  $m_0$  where relic density can be satisfied on the light CP even Higgs pole [35]. This can be seen from Fig.(3) as the gluino and squark masses are exhibited in the plots. Along the Higgs pole region, electroweak symmetry breaking can also be natural, i.e., one has a small  $\mu$ . It is also seen that this region is not constrained by CMS and ATLAS since their limits taper off at large  $m_0$  as  $m_{\text{squark}}$  gets heavy and the jets from squark production are depleted (see Ref. (1) of [34]).

#### IV. CONCLUSION

The CMS and ATLAS analyses on the search for supersymmetry are impressive in that with only  $35 \text{ pb}^{-1}$  of data their reach plots already exceed those from CDF and  $D\bar{O}$  experiments at the Tevatron. Both CMS and ATLAS have given reach plots in the  $m_0 - m_{1/2}$  plane for the case  $A_0 = 0, \tan \beta = 3$  with the ATLAS analysis presenting more stringent limits compared to CMS. Because of the more stringent limits from ATLAS we adopted the ATLAS cuts in our analysis presented in this work. In our analysis we find consistency with the 1 lepton and 0 lepton results of ATLAS for the case analyzed by ATLAS, i.e.,  $A_0 = 0, \tan \beta = 3$ . We have also investigated reach plots for other

values of  $A_0, \tan \beta$ , i.e.,  $A_0 = 0, \tan \beta = 45$  and  $A_0 = 2, \tan \beta = 45$ . Another interesting question explored in this work is a relative study of the constraints on the  $m_0 - m_{1/2}$  parameter space by the CMS and ATLAS experiments vs the constraints that arise from Higgs mass limits, flavor physics, and from the dark matter constraints from WMAP. One finds that the current CMS and ATLAS limits are consistent with such constraints. Specifically a significant part of the parameter space excluded by the CMS and ATLAS 35 pb<sup>-1</sup> data is already excluded by the indirect constraints. We emphasize that low gluino masses (even as low as 400 GeV) remain unconstrained in mSUGRA, and this conclusion holds generically for other high scale models of soft breaking, for the case when the squark masses are significantly larger than the gluino mass. Of interest to the model at hand, is that such situation arises on the hyperbolic branch of radiative breaking of the electroweak symmetry where typically  $\mu$  is relatively small, and the region is very dense in the allowed set of parameter points. Finally, we note that some recent papers related to various topics discussed in this work can be found in Ref.[34].

*Acknowledgements:* PN and GP would like to thank Darien Wood for extended discussions. DF would like to thank Gordy Kane, Katie Freese, Aaron Pierce, and Ran Lu for discussions. NC and ZL thank Jie Chen and Robert Shrock for discussions. This research is supported in part by the Department of Energy (DOE) grant DE-FG02-95ER40899, and the U.S. National Science Foundation (NSF) grants PHY-0757959, and PHY-0969739, and in addition by the NSF TeraGrid resources provided by National Center for Supercomputing Applications (NCSA) under grant number TG-PHY100036.

- 
- [1] A. H. Chamseddine, R. L. Arnowitt and P. Nath, Phys. Rev. Lett. **49**, 970 (1982); P. Nath, R. L. Arnowitt and A. H. Chamseddine, Nucl. Phys. B **227**, 121 (1983).
  - [2] L. J. Hall, J. D. Lykken and S. Weinberg, Phys. Rev. D **27**, 2359 (1983).
  - [3] R. Arnowitt and P. Nath, Phys. Rev. Lett. **69**, 725 (1992).
  - [4] P. Nath, arXiv:hep-ph/0307123; P. Nath, R. L. Arnowitt, A. H. Chamseddine, “Applied N=1 Supergravity,” World Scientific Singapore, 1984; H. P. Nilles, Phys. Rept. **110**, 1-162 (1984); L. E. Ibanez and G. G. Ross, Comptes Rendus Physique **8**, 1013 (2007).
  - [5] G. Kane et. al “Perspectives on supersymmetry. Vol.2,” *World Scientific (2010) 583 p.*
  - [6] P. Nath, B. D. Nelson, D. Feldman, Z. Liu *et al.*, Nucl. Phys. Proc. Suppl. **200-202**, 185 (2010).
  - [7] V. Khachatryan *et al.* [CMS Collaboration], arXiv:1101.1628 [hep-ex].
  - [8] T. A. Collaboration, arXiv:1102.2357 [hep-ex].
  - [9] T. A. Collaboration, arXiv:1102.5290 [hep-ex].
  - [10] For a review of LEP/Tevatron constraints see: J. L. Feng, J. F. Grivaz and J. Nachtman in Ref. [5] and Rev. Mod. Phys. **82**, 699 (2010).
  - [11] D. Feldman, Z. Liu and P. Nath, Phys. Rev. Lett. **99**, 251802 (2007); Phys. Lett. B **662**, 190 (2008); JHEP **0804**, 054 (2008); Phys. Rev. D **80**, 015007 (2009); Phys. Rev. D **81**, 095009 (2010).
  - [12] H. Baer, V. Barger, A. Lessa and X. Tata, JHEP **1006**, 102 (2010).
  - [13] B. Altunkaynak, M. Holmes, P. Nath, B. D. Nelson, G. Peim, Phys. Rev. D **82**, 115001 (2010).
  - [14] N. Chen, D. Feldman, Z. Liu, P. Nath, G. Peim, arXiv:1011.1246 [hep-ph], Phys. Rev. D **83**, 035005 (2011); N. Chen et al., Phys. Rev. D **83**, 023506 (2011).
  - [15] D. Feldman, G. Kane, R. Lu and B. D. Nelson, Phys. Lett. B **687**, 363 (2010); G. L. Kane, E. Kuflik, R. Lu and L. T. Wang, arXiv:1101.1963 [hep-ph].
  - [16] E. Izaguirre, M. Manhart and J. G. Wacker, JHEP **1012**, 030 (2010); D. S. M. Alves, E. Izaguirre and J. G. Wacker, arXiv:1008.0407 [hep-ph].
  - [17] J. Alwall *et al.*, JHEP **0709**, 028 (2007);
  - [18] T. Sjostrand, S. Mrenna and P. Z. Skands, JHEP **0605**, 026 (2006).
  - [19] R. Barate *et al.* [Phys. Lett. B **565**, 61 (2003).
  - [20] [CDF and D0 Collaboration], arXiv:1007.4587 [hep-ex].
  - [21] G. Belanger, F. Boudjema, P. Brun, A. Pukhov, S. Rosier-Lees, P. Salati and A. Semenov, Comput. Phys. Commun. **182**, 842 (2011).
  - [22] A. Djouadi, J. L. Kneur and G. Moultaka, Comput. Phys. Commun. **176**, 426 (2007).
  - [23] M. Muhlleitner, A. Djouadi and Y. Mambrini, Comput. Phys. Commun. **168**, 46 (2005); A. Djouadi, M. M. Muhlleitner and M. Spira, Acta Phys. Polon. B **38**, 635 (2007).
  - [24] K. Nakamura *et al.* [Particle Data Group Collaboration], J. Phys. G **G37**, 075021 (2010).
  - [25] [http://atlas.web.cern.ch/Atlas/GROUPS/PHYSICS/PAPERS/susy-01epton\\_01/](http://atlas.web.cern.ch/Atlas/GROUPS/PHYSICS/PAPERS/susy-01epton_01/)
  - [26] A. Djouadi, M. Drees and J. L. Kneur, JHEP **0603**, 033 (2006).
  - [27] E. Barberio *et al.* [Heavy Flavor Averaging Group], arXiv:0808.1297 [hep-ex].
  - [28] N. Chen, D. Feldman, Z. Liu and P. Nath, Phys. Lett. B **685**, 174 (2010).
  - [29] T. Aaltonen *et al.* [CDF Collaboration], Phys. Rev. Lett. **100**, 101802 (2008).

- [30] M. Misiak *et al.*, Phys. Rev. Lett. **98**, 022002 (2007).
- [31] E. Komatsu *et al.* [WMAP Collaboration], Astrophys. J. Suppl. **192**, 18 (2011); N. Jarosik *et al.*, [arXiv: 1001.4744 [astro-ph.CO]]; D. N. Spergel *et al.*, Astrophys. J. Suppl. **170**, 377 (2007); Astrophys. J. Suppl. **148**, 175 (2003).
- [32] G. Aad *et al.* [ The ATLAS Collaboration ],
- [33] K. L. Chan, U. Chattopadhyay and P. Nath, Phys. Rev. D **58** (1998) 096004; R. L. Arnowitt and P. Nath, Phys. Rev. D **46**, 3981 (1992); J. L. Feng, K. T. Matchev and T. Moroi, Phys. Rev. Lett. **84**, 2322 (2000); U. Chattopadhyay, A. Corsetti and P. Nath, Phys. Rev. D **68**, 035005 (2003); H. Baer, C. Balazs, A. Belyaev, T. Krupovnickas and X. Tata, JHEP **0306**, 054 (2003); D. Feldman, Z. Liu and P. Nath, Phys. Rev. D **78**, 083523 (2008); S. Cassel, D. M. Ghilencea, S. Kraml, A. Lessa, G. G. Ross, [arXiv:1101.4664 [hep-ph]].
- [34] D. Feldman, K. Freese, P. Nath, B. D. Nelson, G. Peim, [arXiv:1102.2548 [hep-ph]]; I. Gogoladze, R. Khalid, S. Raza, Q. Shafi, [arXiv:1102.0013 [hep-ph]]; B. C. Allanach, [arXiv:1102.3149 [hep-ph]]; H. K. Dreiner, S. Grab, T. Stefaniak, [arXiv:1102.3189 [hep-ph]]; S. Scopel, S. Choi, N. Fornengo, A. Bottino, [arXiv:1102.4033 [hep-ph]]; O. Buchmueller et.al., [arXiv:1102.4585 [hep-ph]]; M. Guchait and D. Sengupta, arXiv:1102.4785 [hep-ph]; P. Bechtle et.al., [arXiv:1102.4693 [hep-ph]]; D. S. M. Alves, E. Izaguirre, J. G. Wacker, [arXiv:1102.5338 [hep-ph]]; B. C. Allanach, T. J. Khoo, C. G. Lester and S. L. Williams, arXiv:1103.0969 [hep-ph].
- [35] P. Nath, R. L. Arnowitt, Phys. Rev. Lett. **70**, 3696-3699 (1993). [hep-ph/9302318].